Check for updates

AGU ADVANCING EARTH AND SPACE SCIENCE

Geophysical Research Letters

RESEARCH LETTER
10.1029/2020GL088797

# Flood Variability Determines the Location of Lobe-Scale Avulsions on Deltas: Madagascar

**Sam A. S. Brooke[1], Vamsi Ganti[1,2], Austin J. Chadwick[3], and Michael P. Lamb[4]**

[1]Department of Geography, University of California Santa Barbara, Santa Barbara, CA, USA, [2]Department of Earth Science, University of California Santa Barbara, Santa Barbara, CA, USA, [3]Department of Earth Sciences and St. Anthony Falls Laboratory, University of Minnesota, Minneapolis, MN, USA, [4]Division of Geological and Planetary Sciences, California Institute of Technology, Pasadena, CA, USA

**Key Points:**
- Using Landsat imagery spanning 1978 to 2019 CE, we identified two lobe-scale fan and five delta avulsions on the western coast of Madascagar
- Unlike low-gradient rivers, delta avulsion lengths in steep, silt-bedded rivers of Madagascar are much longer than the backwater lengthscale
- Avulsion sites scale with expected length of the flood-induced scour zone, bolstering the backwater hypothesis for avulsions

**Supporting Information:**
- Supporting Information S1
- Table S1
- Table S2

**Correspondence to:**
S. A. S. Brooke,
sbrooke@ucsb.edu

**Citation:**
Brooke, S. A. S., Ganti, V., Chadwick, A. J., & Lamb, M. P. (2020). Flood variability determines the location of lobe-scale avulsions on deltas: Madagascar. *Geophysical Research Letters*, *47*, e2020GL088797. https://doi.org/10.1029/2020GL088797

Received 14 MAY 2020
Accepted 16 SEP 2020
Accepted article online 21 SEP 2020

**Abstract** River deltas grow through repeated lobe-scale avulsions, which often occur at a location that correlates with the backwater lengthscale. Competing hypotheses attribute the avulsion node origin to either the morphodynamic feedbacks caused by natural flood discharge variability (backwater hypothesis) or to the prograding delta lobe geometry (geometric hypothesis). Here, using theory, historical flood records, and remotely sensed elevation data, we analyzed five lobe-scale delta avulsions in Madagascar, captured by Landsat imagery. Avulsion lengths were 5–55 km, distances significantly longer than the backwater lengthscale and inconsistent with the geometric hypothesis. We show that the steep, silt-bedded rivers of Madagascar have flood-induced bed scour, driven by backwater hydrodynamics, that propagates farther upstream than the backwater lengthscale. The avulsion lengths are $3.1 \pm 1.5$ times the predicted flood scour lengths, similar to low-gradient deltas, and consistent with backwater hypothesis. Results demonstrate that erosion initiated by nonuniform flows in the backwater zone is a primary control on delta avulsion locations.

**Plain Language Summary** River deltas grow through abrupt channel shifts, called avulsions, which pose a threat to life and property, but we do not understand why avulsions occur where they do. One hypothesis is that flood discharge variability creates a preferential zone of sediment accumulation within the so-called backwater zone of coastal rivers, which becomes the locus of avulsion. The rationale is that the flow acceleration and deceleration within the backwater zone during different sized floods creates nonoverlapping patterns of erosion and deposition resulting in a peak in sediment accumulation. If this hypothesis is correct, then avulsion sites should be farther upstream, relative to the backwater lengthscale, in steep rivers with fine-grained sediment beds that have more significant bed scour during large floods. By analyzing historical avulsions on Madagascar, we found that avulsions occurred far upstream due to the large floods and fine-grained sediment, in support of the flood discharge variability hypothesis. Our work highlights that changes in flood regime and sediment grain size of coastal rivers due to land use and climate changes can influence avulsion location.

## 1. Introduction

Sudden shifts in a river course—or avulsions—are natural phenomena that occur on alluvial fans and river deltas (Blair & McPherson, 1994; Jerolmack, 2009; Jones & Schumm, 1999; Slingerland & Smith, 2004). Avulsions are an essential formative process in fan and delta evolution, where repeated lobe-scale channel jumps change the downstream loci of sedimentation to produce a characteristic radial pattern of distinct lobes about a spatial node (Figure 1a; Jerolmack, 2009). Avulsions represent a significant geohazard to the hundreds of millions of people living in the proximity of rivers (Kidder & Liu, 2017; Sinha, 2009; Syvitski & Brakenridge, 2013; Syvitski & Saito, 2007). A mechanistic understanding of the processes that culminate in lobe-scale river avulsions has wide-ranging implications for flood risk management, coastal sustainability, and the interpretation of fluvial stratigraphy (Bull, 1977; Ganti et al., 2019; Jones & Hajek, 2007; Mohrig et al., 2000; Syvitski et al., 2009; Törnqvist, 1994; Trower et al., 2018). Further, climate change and human activity are forecasted to alter flood frequency, relative sea level, and the amount and caliber of sediment supply (Best & Darby, 2020; Hirabayashi et al., 2013); however, their impact on river avulsions is unclear (Chadwick et al., 2020).

©2020. American Geophysical Union. All Rights Reserved.

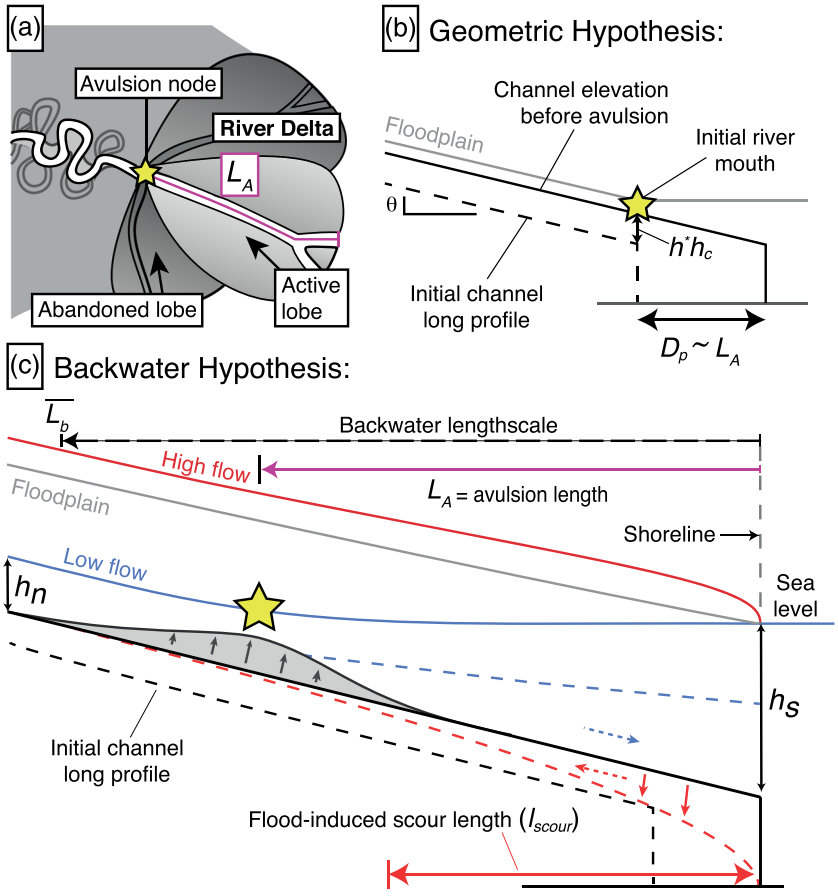


**Figure 1.** (a) Schematic river delta built through cycles of lobe-scale avulsions that occur at a predictable distance upstream from the river mouth ($L_A$). (b) Under the geometric hypothesis, $L_A$ scales with the typical progradation length, $D_p$, during the interavulsion period, which correlates with the backwater lengthscale, $\overline{L_b}$ (Equation 3). The avulsion threshold ($h^*$) is achieved at the river mouth of the initial channel bed profile (yellow star) where a floodplain gradient break exists because the new delta lobe floodplain elevation is near sea level. (c) Under the backwater hypothesis, the preferred avulsion location (yellow star) arises from natural flood discharge variability. Low flows (blue water surface profile) drive a downstream-migrating wave of deposition (blue dashed line) within the backwater zone; however, floods (red water surface profile) cause an upstream-migrating wave of erosion (dashed red line) with a typical lengthscale of $l_{scour}$. Riverbed aggradation is maximized upstream of the flood scour zone over multiple flood cycles.

Avulsions are driven by preferential riverbed aggradation that, over time, renders the channel unstable and prone to an avulsion (Mohrig et al., 2000; Slingerland & Smith, 2004). Previous work suggests that the controls on avulsions for alluvial fans and river deltas are different (Ganti et al., 2014). Unlike steep alluvial fans, most lowland delta avulsions are not coincident with an abrupt change in channel gradient or valley confinement (Ganti et al., 2014). Instead, delta avulsions occur at a statistically predictable distance upstream of the shoreline ($L_A$) that scales with the backwater lengthscale ($\overline{L_b}$) (Chatanantavet et al., 2012; Jerolmack & Swenson, 2007), in which $\overline{L_b} = h_c/S$ (Paola & Mohrig, 1996), where $h_c$ and $S$ are the bankfull flow depth and channel bed slope, respectively. One hypothesis for the origin of the correlation of $\overline{L_b} \sim L_A$ relates to the geometry of prograding delta lobes (Chadwick et al., 2019; Ratliff, 2017). Under this hypothesis, lobes must prograde a distance of about $\overline{L_b}$ to aggrade a critical amount for an avulsion, which scales with $h_c$ (Mohrig et al., 2000), assuming that floodplain is near sea level (Figure 1b; Chadwick et al., 2019; Ratliff, 2017). In contrast, other numerical (Chadwick et al., 2019; Chatanantavet et al., 2012; Moodie et al., 2019) and experimental (Ganti, Chadwick, Hassenruck-Gudipati, Fuller, et al., 2016; Ganti, Chadwick, Hassenruck-Gudipati, & Lamb, 2016) models assume floodplains aggrade with the riverbed,

and argue instead that the preferential avulsion site emerges from natural flood discharge variability and backwater hydrodynamics. Under the backwater hypothesis, low flows and floods cause sedimentation and erosion within the upstream and downstream part of the backwater zone, respectively (Figure 1c) (Chatanantavet & Lamb, 2014; Lamb et al., 2012), causing enhanced deposition and avulsions with $\overline{L_b}$~$L_A$ because $\overline{L_b}$ approximates the upstream extent of nonuniform flows (Lamb et al., 2012).

For most lowland deltas $L_A$ scales with $\overline{L_b}$ within a factor of 2 (Chatanantavet et al., 2012; Jerolmack & Swenson, 2007). Thus, it is difficult to separate the competing influence of geometric effects from backwater effects—both processes cause $L_A$~$\overline{L_b}$. Previous work was focused on numerical models and flume experiments to isolate the driving mechanism for delta avulsions (Chadwick et al., 2019; Ganti, Chadwick, Hassenruck-Gudipati, Fuller, et al., 2016; Ganti, Chadwick, Hassenruck-Gudipati, & Lamb, 2016). However, theory indicates that backwater-induced nonuniform flows can extend to upstream distances longer than $\overline{L_b}$ for coastal rivers with unusually high flood discharge variability (Lamb et al., 2012). Similarly, flood-induced scours might propagate beyond $\overline{L_b}$ for coastal rivers with steep gradients and fine bed material (Chadwick et al., 2019; Ganti et al., 2019) that cause high sediment fluxes (Ma et al., 2017), or for long-duration floods (Chatanantavet & Lamb, 2014). Thus, under the backwater hypothesis, $L_A$ might significantly exceed $\overline{L_b}$ in specific rivers with steep slopes, sustained floods, high flood variability, or fine sediment that results in large sediment fluxes. Identifying such avulsions would provide a robust test of competing hypotheses for the origin of delta avulsions.

Here, we used Landsat imagery, remotely sensed elevation data, and historical flood records to document avulsions in Madagascar. Madagascan rivers have steep slopes, large fine-grained sediment supply, and a monsoonal hydroclimate, making them an ideal place to evaluate the competing hypotheses for avulsions.

## 2. Theory

### 2.1. Backwater Controls on Delta Avulsions

Under the backwater hypothesis, avulsions are driven by the morphodynamic feedbacks initiated by the nonuniform flows caused by variable flood discharges and the influence of sea level (Figure 1c; Chatanantavet et al., 2012). The upstream extent of these nonuniform flows is (Bresse, 1860; Text S1 in the supporting information):

$$\frac{L_b}{\overline{L_b}} = f\left(Fr, \frac{h_s}{h_n}\right) \tag{1}$$

where $L_b$ is the backwater or drawdown length, $Fr$ is the Froude number, $h_s$ is the flow depth at the river mouth, and $h_n$ is the normal flow depth of a given flood (Figure 1c). When $h_s > h_n$, flow decelerates toward the shoreline causing sedimentation; however, when $h_s < h_n$, flow accelerates toward the shoreline causing an upstream-migrating wave of erosion (Chatanantavet & Lamb, 2014; Lamb et al., 2012). For rivers with high flood discharge variability, $h_s$ and $h_n$ can be significantly different such that $L_b \approx \overline{L_b}$ during floods (Lamb et al., 2012).

Using a numerical model, Chadwick et al. (2019) identified the duration of a typical flood ($t_{scour}$), relative to the channel bed adjustment time scale ($t_{adj} = h_c\overline{L_b}/q_s$ where $q_s$ is the unit volumetric sediment flux; Chatanantavet & Lamb, 2014), as a fundamental control on avulsions, parameterized by the dimensionless number: $T_e^* = t_{scour}q_s/h_c\overline{L_b}$. Numerical results indicated that $L_A$~$\overline{L_b}$ only for rivers with $T_e^* \in [10^{-4}, 10^{-1}]$ such that the backwater-induced sedimentation and erosion patterns were limited to the backwater zone (Figure 1c). In contrast, avulsion lengths were longer than $\overline{L_b}$ for $T_e^* > 1$ (Chadwick et al., 2019). Long flood durations, relative to $t_{adj}$, cause the equilibration of riverbed topography and the flood event across the entire backwater zone such that the preferential avulsion location shifts farther upstream (Figure 1c).

The lengthscale over which erosional scours propagate upstream of the river mouth during typical floods ($l_{scour}$) represents a lower bound on $L_A$ as riverbed aggradation is maximized upstream of the flood scour zone during the interavulsion period (Figure 1c; Chadwick et al., 2019; Chatanantavet et al., 2012; Ganti, Chadwick, Hassenruck-Gudipati, Fuller, et al., 2016; Ganti, Chadwick, Hassenruck-Gudipati, & Lamb, 2016). Ganti et al. (2019) developed a framework for estimating $l_{scour}$ in sand-bedded rivers,

which we extended to include silt-bedded rivers using the generalized Enguland-Hansen relation for sediment transport capacity (Ma et al., 2017, 2020) to yield:

$$\frac{l_{scour}}{\overline{L_b}} = \sqrt{T_e^*} = \left[ t_{scour} \frac{\sqrt{(RgD_{50}^3)}\alpha(h_n S)^n}{h_c \overline{L_b} C_f (RD_{50})^n} \right]^{0.5} \quad (2)$$

where $h_n$ is the normal-flow depth of a typical flood, $D_{50}$ is the median bed material grain size, $R = 1.65$ is the submerged specific gravity of sediment for quartz, $g$ is the gravitational acceleration, $C_f$ is a dimensionless friction coefficient, $\alpha$ and $n$ are grain size-dependent empirical constants (Text S2). Consistent with numerical simulations (Chadwick et al., 2019), Equation 2 predicts that $L_A > \overline{L_b}$ for rivers with $T_e^* > 1$ because $l_{scour} > \overline{L_b}$.

### 2.2. Geometric Controls on Delta Avulsions

In contrast to the backwater hypothesis, previous work indicated that $L_A$ can correlate with $\overline{L_b}$ without the need for flood discharge variability (Chadwick et al., 2019; Moran et al., 2017; Ratliff, 2017). Under this geometric hypothesis, river mouth progradation causes riverbed aggradation, and in the absence of relative sea level rise, a riverbed with a constant slope must prograde by a distance of $h_c/S$ before it aggrades by $h_c$ (e.g., Ganti et al., 2014; Paola, 2000; Reitz et al., 2015). Insofar as the critical amount of riverbed aggradation necessary for an avulsion scales with $h_c$, avulsions should occur when the delta lobe progrades by a distance that scales with the backwater lengthscale, that is, $\overline{L_b} = h_c/S$ (Figure 1b). Numerical models indicate that this correlation arises only when the floodplain does not aggrade with the riverbed (Chadwick et al., 2019), and the floodplain elevation on the newly constructed delta lobe is constrained at or near sea level (Figure 1b; Ratliff, 2017; Ratliff et al., 2018). This mechanism causes a floodplain gradient break between the initial and the new delta lobe surfaces such that the riverbed is steeper than the floodplain at all locations downstream of the avulsion site, and the critical channel superelevation necessary for an avulsion is first achieved at the river mouth of the initial channel profile (Figure 1b).

Under this hypothesis, $L_A$ scales with the typical delta lobe progradation length, $D_p$, during the interavulsion period, which, by geometry is (Ganti et al., 2019):

$$D_p = \left(h^* - {}^{z}/_{h_c}\right)\overline{L_b} \quad (3)$$

where $h^*$ is the avulsion threshold—the critical fraction of $h_c$ a channel needs to aggrade before avulsion—and $z$ is the amount of base-level rise during the interavulsion period. Field observations indicate that $h^* \in [0.2, 1.4]$ (Ganti et al., 2014, 2019; Mohrig et al., 2000) such that $D_p \sim \overline{L_b}$ for modest rates of relative base-level rise. Geometric avulsion lengths increase with avulsion threshold and decrease with sea level rise (Equation 3; Ratliff, 2017; Chadwick et al., 2019).

The backwater and geometric hypotheses for delta avulsions provide contrasting predictions for avulsion locations on steep coastal rivers with sustained floods. Equation 2 indicates that $L_A$, and consequently delta size, can be significantly longer than $\overline{L_b}$ for rivers with $T_e^* > 1$. In contrast, Equation 3 indicates that $L_A \sim \overline{L_b}$ regardless of the prevailing flood regime. We test these theoretical predictions by exploring the controls on avulsions in Madagascar.

## 3. Study Area: Madagascar

Madagascar is the world's fourth largest island, with intense soil erosion due to the exposed saprolitic soils, rapid deforestation, and land use changes (Randrianarijaona, 1983; Unruh et al., 2010), resulting in, potentially, the world's highest erosion rates (World Bank et al., 1988). Hillslope gullying, called Lavakas ("hole" in Malagasy), are abundant in Madagascar's hinterland (Cox et al., 2010; Voarintsoa et al., 2012; Wells & Andriamihaja, 1993), feeding its rivers with ~30 t km$^2$ yr$^{-1}$ of fine-grained material exhumed from 3- to 30-m-deep incisions (Cox et al., 2009). The largest rivers in Madagascar are westward flowing and drain the interior highlands with an elevation change of 1–2 km between headwater and river mouth.

The high fluvial sediment supply causes high sedimentation rates and frequent avulsions that are observable in the Landsat data.

Madagascar is a tropical island, subclassified into a drier subtropical south and a monsoonal north, with average monthly precipitation ranging from 200–300 mm on the eastern rainforest-covered flank to 100–150 mm in the northern and central interior (Fick & Hijmans, 2017, Figure S1a). Tropical storms frequently impact the northwestern region, where daily rainfall can exceed 70 mm (Nassor & Jury, 1997, 1998). The rivers exhibit a highly seasonal discharge regime, with peak floods during December to March (Figure S2). The high, fine-grained sediment supply and prolonged flood seasons of Madagascar favor large flood-induced bed scour lengths that potentially exceed $\overline{L_b}$ (Equation 2).

The wave heights on the western coast of Madagascar vary from 0.2 to 0.75 m (Nienhuis et al., 2020). Of the five deltas analyzed here, two were classified as river dominated (Mangoky and Sambao) and three as wave dominated (Morandava, Manambolo, Fiherenana) (Nienhuis et al., 2020), in which coastal wave erosion likely limits lobe progradation rates (Ashton & Giosan, 2011; Ratliff et al., 2018).

## 4. Methods

We located lobe-scale avulsions in Madagascar through (a) time series analysis of net surface water changes derived from Landsat multispectral data between 1984 and 2018 CE (Figure S3; Pekel et al., 2016) and (b) visual comparison of river path changes from 30 m spatial resolution Landsat imagery available between 1978 and 2019 CE (Figure 2). We identified lobe-scale avulsions as a permanent change in the river course (Figure S3), including both gradual and abrupt avulsions (Figure 2). We excluded intralobe avulsions from our analysis (Figure 2b). For all avulsions, we computed $L_A$ as the streamwise distance from the river mouth to the avulsion site, using the Landsat image that best captured the time of avulsion (Figure 2). The avulsion sites were stable during the channel relocation process, yielding an uncertainty of one channel width on $L_A$. We also identified an avulsion that predated the Landsat data on the Mangoky delta, where the former and current river paths are apparent (Figure 2b).

For all avulsions, we extracted the river long profiles from the 30 m spatial resolution SRTM digital elevation model collected in 2000 CE. We used orthogonal transects of the channel, including the adjacent floodplain at 10 m intervals upstream as a means to mitigate surface model artifacts on water bodies, or where rivers are monotonically stepped as part of SRTM postprocessing. These transects extended 100–1,000 m across the active floodplain, depending on the valley width, and reliably captured the downstream elevation change. We measured channel slopes over nonoverlapping 5 km windows, binned every 25 km (Figures S4 and S5).

To compare to theory, we estimated the bankfull flow depth ($h_c$) of the Madagascan rivers upstream of the avulsion sites using empirical scaling relations (Text S3). The bed material load of the westward draining Madagascan rivers is unusually fine and dominated by suspended sediment with a median grain diameter of 60 to 90 μm (Bresson, 1956; Walling, 1984), similar to the Huanghe (Moodie et al., 2019). We assumed $D_{50} = 90$ μm for the Madagascan rivers and estimated $h_c$ using the empirical bankfull Shields stress relation (Trampush et al., 2014) and the threshold channel theory for alluvial rivers (Dunne & Jerolmack, 2018). These independent methods yielded consistent $h_c$ values.

We computed $\overline{L_b}$ using the $h_c$ estimates and $S$, evaluated upstream of the avulsion site. We evaluated $L_b/\overline{L_b}$ (Equation 1; Text S1) for the Mangoky River, where all relavant parameters could be constrained. We assumed this ratio to be representative of all Madagascan rivers analyzed here. We compiled monthly flood discharge time series for all available Madasgacan rivers (GRDC, 2015; Vorosmarty et al., 1998; Figure S1). In Equation 1, we assumed that the flow depth at the shoreline ($h_s$) was equal to $h_c$, and $h_s/h_n = 0.33$ for typical floods (Ganti et al., 2014; Gibling, 2006). For low flows, we assumed $h_s/h_n = (Q_{bf}/Q_{low})^{2/3}$ following the Manning-Strickler relation, where $Q_{bf}$ is the bankfull water discharge—equated to the 2-year recurrence interval flood—and $Q_{low}$ is the minimum recorded water discharge. Depth-averaged flow velocities of $U \approx 1$ m/s were measured during bankfull floods on the Mangoky River (Bresson, 1956), and we evaluated $Fr = U/\sqrt{gh_c}$.

Erosional scours occur during floods that exceed $Q_{bf}$ (Lamb et al., 2012). To evaluate $l_{scour}$ (Equation 2), we equated $t_{scour}$ to the continuous duration for which flow exceeded $Q_{bf}$ in the monthly discharge time series.

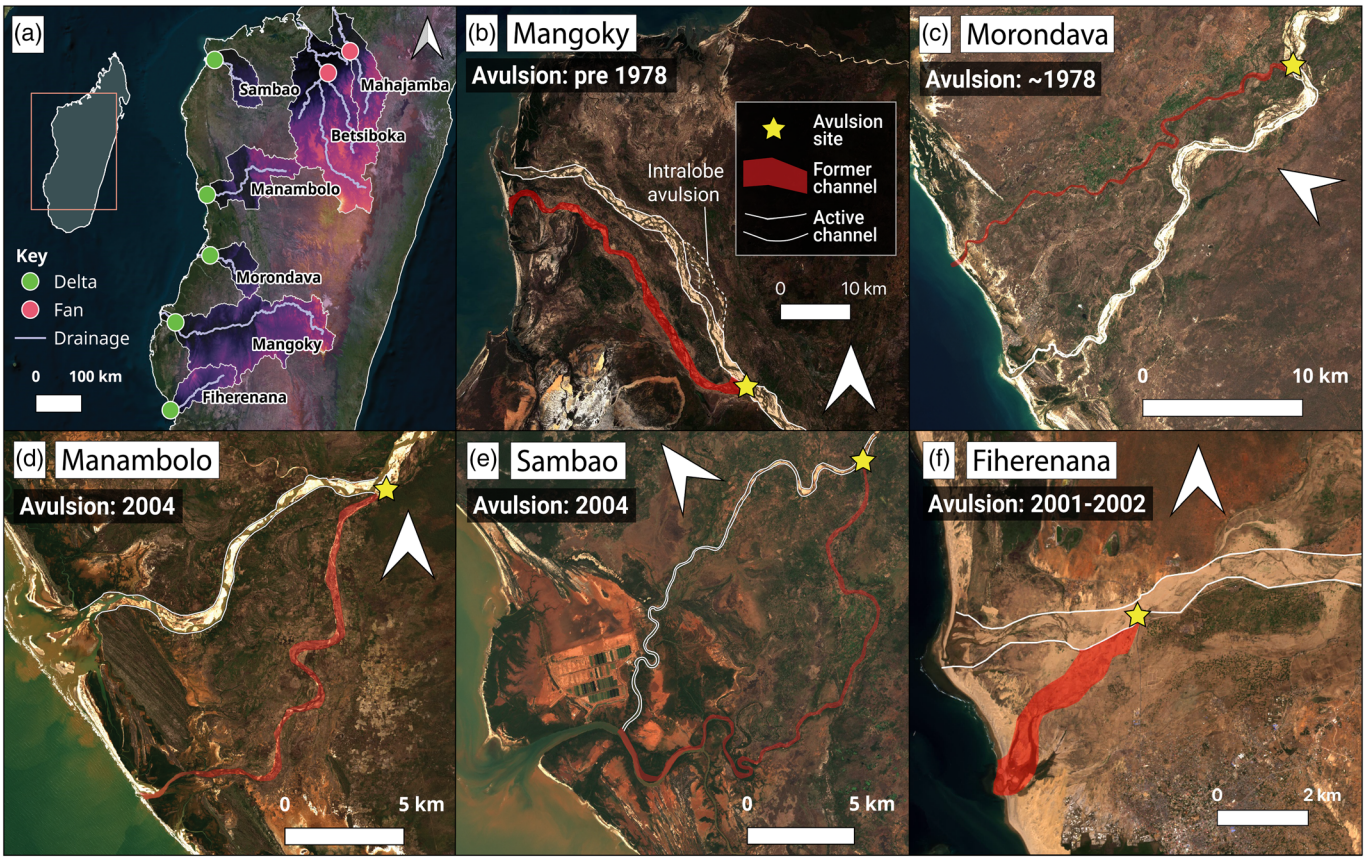


**Figure 2.** (a) Lobe-scale avulsion sites in Madagascar (inset). (b–f) ESA Sentinel 2 bottom-of-atmosphere-corrected optical imagery of avulsion sites on deltas (yellow stars), with the former and current river course outlined by red semitransparent polygon and white lines, respectively.

Data were available for three of the five rivers studied here, and where data were unavailable, we used proximal gauge station data assuming discharge regime scales with local precipitation pattern (Table S1; Figure S1). In Equation 2, we evaluated $C_f = gh_c S/U^2 \approx 0.01$ for the Mangoky River, and assumed the same $C_f$ for all Madagascan rivers.

We also evaluated $l_{scour}$ for a representative global compilation of low-gradient, coastal rivers (Chatanantavet et al., 2012; Ganti et al., 2014; Moodie et al., 2019). For this compilation, we identified the closest river gauge to the avulsion site and evaluated $t_{scour}$ as the duration for which flow exceeded the reported $Q_{bf}$. We used monthly discharge time series, and estimated $l_{scour}$ for rivers using both daily and montly discharge data when both data sets were available. These estimates showed good agreement (Figure S6). All other parameters in Equation 2 were reported in previous studies (Table S2). We quantified uncertainty in $\overline{L_b}$ and $l_{scour}$ using Monte Carlo simulations ($n$ = 20,000), and the evaluation of parameter uncertainty is summarized in text S5. We report the mean and standard deviation of $\overline{L_b}$ and $l_{scour}$ derived from the Monte Carlo simulations.

Finally, to compare $L_A$ with predictions of the geometric hypothesis (equation 3), we evaluated the maximum progradation length of delta lobes by setting $z = 0$ and $h^* \in [0.2, 1.4]$, consistent with observations of avulsion thresholds in modern and ancient environments (Ganti et al., 2014, 2019; Mohrig et al., 2000).

## 5. Results

We observed seven lobe-scale avulsions on the western coast of Madagascar (Figures 2 and S7). Of these, two avulsions occurred farther inland on the Betsiboka and Mahajamba Rivers (Figure 2a), coincident with an

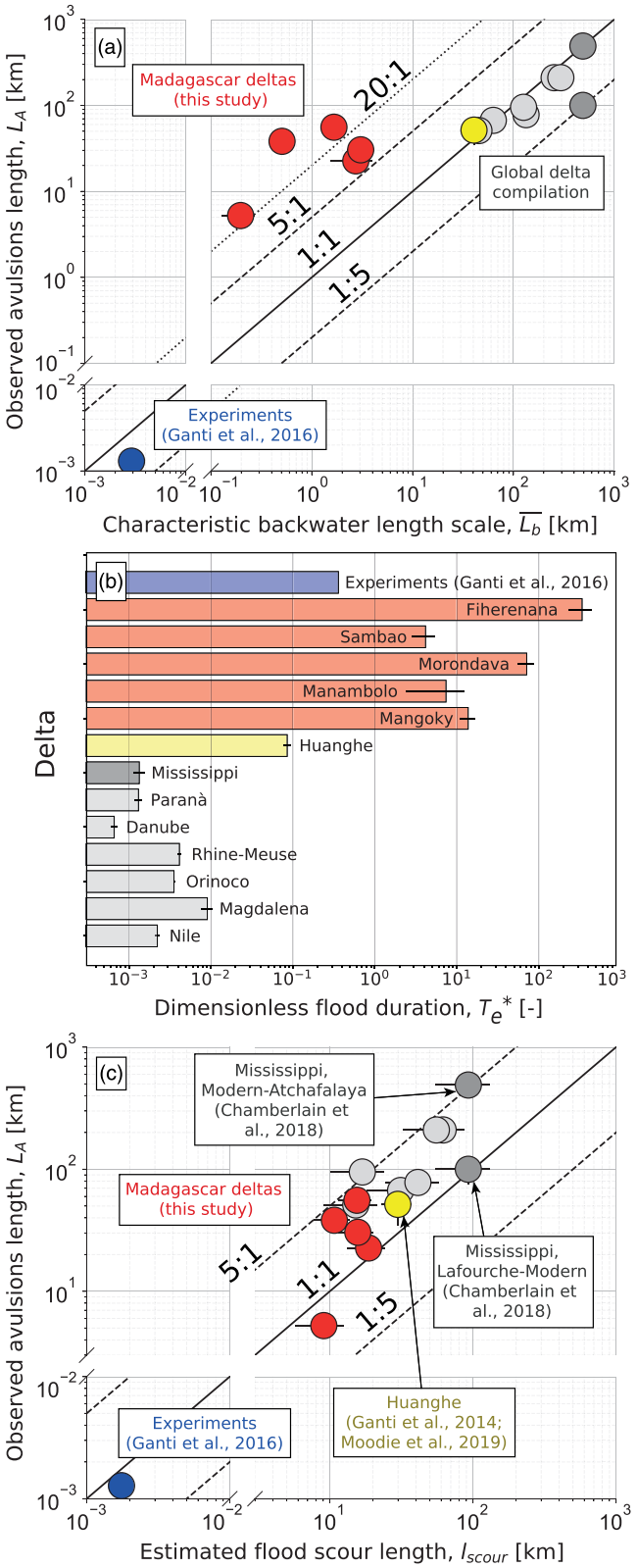


**Figure 3.** Observed avulsion length ($L_A$) as a function of the (a) backwater lengthscale ($\overline{L_b}$) and (c) estimated flood-scour length ($l_{scour}$; Equation 2) for the Madagascan rivers (red), Huanghe (yellow), Lower Mississippi (dark gray), low-gradient delta compilation (Chatanantavet et al., 2012; Ganti et al., 2014; Moodie et al., 2019), and the backwater-scaled delta experiment (Ganti, Chadwick, Hassenruck-Gudipati, Fuller, et al., 2016; Ganti, Chadwick, Hassenruck-Gudipati, & Lamb, 2016). (b) Computed dimensionless flood duration, $T_e^*$, across natural and experimental deltas.

abrupt channel gradient break (Text S4 and Figure S7), and consistent with processes that cause avulsions on alluvial fans (Ganti et al., 2014; Hartley et al., 2017; Jones & Schumm, 1999; Slingerland & Smith, 2004).

We also located five lobe-scale delta avulsions on the Sambao, Manambolo, Morondava, Fiherenana, and Mangoky Rivers (Figure 2), which are not coincident with a distinctive change in valley confinement or channel gradient (Figure S4). The observed avulsion lengths, $L_A$, ranged from 5.2 km (Fiherenana) to 55.8 km (Mangoky)—distances significantly longer than $\overline{L_b}$ of 0.20 ± 0.07 km (Fiherenana) to 3.07 ± 0.80 km (Sambao) (Figure 3a). The estimated backwater and drawdown lengths were $0.98\overline{L_b}$ (Fr = 0.3, $h_s/h_n = 9$; Text S1) and $1.3\overline{L_b}$ (Fr = 0.3, $h_s/h_n = 0.33$; Text S1), respectively, indicating that the lengthscale of the zone of nonuniform flows is much shorter than the observed avulsion lengths (Figure 3a). In contrast, $L_A$ scales with $\overline{L_b}$ for the compilation of low-gradient coastal rivers ($\overline{L_b}/L_A = 1.57 \pm 0.43$ (mean ± standard error, S.E.); Chatanantavet et al., 2012; Jerolmack & Swenson, 2007); whereas $\overline{L_b}/L_A = 0.06 \pm 0.02$ is far smaller for the Madagascan rivers (Figure 3a).

The average $t_{scour}$ value for the Madagascan rivers ranged from 1.3 to 1.7 months, similar to other low-gradient rivers (Table S1). However, the dimensionless flood duration, $T_e^*$, was orders-of-magnitude different for the Madagascan rivers owing to their short channel bed adjustment time scales caused by the exceptional sediment load of steep, fine-grained rivers (Figure 3b). The $T_e^*$ value was order $10^1$ for Mangoky, Sambao, and Manambolo and $10^2$ for Fiherenana and Morondava (Figure 3b). In contrast, $T_e^*$ was order $10^{-3}$ to $10^{-2}$ for other low-gradient, sand-bedded rivers (Mississippi, Orinoco, Danube) and $10^{-1}$ for the Huanghe—a silt-bedded, low-gradient river (Figure 3b). The high $T_e^*$ values of the Madagascan rivers resulted in $l_{scour} > \overline{L_b}$ (Equation 2). For example, $l_{scour}$ for the Sambao and Manambolo Rivers were 15.7 ± 4.34 km and 18.65 ± 5.44 km—values significantly longer than their $\overline{L_b}$ of 3.07 ± 0.80 km and 2.73 ± 1.22 km, respectively.

Results show that $l_{scour}$ scales with $L_A$ for the Madagascan rivers, consistent with backwater hypothesis for avulsions and with the compilation of other low-gradient rivers (Chadwick et al., 2019; Chatanantavet et al., 2012; Ganti, Chadwick, Hassenruck-Gudipati, Fuller, et al., 2016; Ganti, Chadwick, Hassenruck-Gudipati, & Lamb, 2016) (Figure 3c). Under the backwater hypothesis, riverbed aggradation, and consequently the propensity for avulsions, is limited within the flood scour zone because bankfull-exceeding floods cause erosion during the interavulsion period (Figure 1c). Experiments and theory indicate that the riverbed aggradation is maximized upstream of the flood scour zone (Figure 1c; Chadwick et al., 2019; Chatanantavet et al., 2012; Ganti, Chadwick, Hassenruck-Gudipati, Fuller, et al., 2016; Ganti, Chadwick, Hassenruck-Gudipati, & Lamb, 2016), and $l_{scour}$ is a first-order estimate of $L_A$. In our compilation (Figure 3c), only the Fiherenana avulsion occurred within the predicted flood scour zone. The estimated $l_{scour}$ for the Fiherenana had significant uncertainty as it lacked a gauged discharge record, and we estimated $t_{scour}$ from a proximal river gauge station (Mangoky) (Figure S1b). The ratio of $l_{scour}$ to $L_A$ for the Madagascan rivers is 0.73 ± 0.27 (mean ± S.E.) and 0.47 ± 0.13, including and excluding the Fiherenana, respectively, consistent with the global low-gradient delta compilation ($l_{scour}/L_A = 0.41 \pm 0.08$).

The avulsion lengths on Madagascan deltas are inconsistent with the geometric hypothesis (Equation 3; Figure 1b). Under this hypothesis, $L_A$ should scale with $D_p$ (Equation 3) because this amount of delta lobe progradation will cause the critical sedimentation necessary for an avulsion (Figure 1b). For $h^* \in [0.2, 1.4]$, maximum $D_p$ is $0.2\overline{L_b}$ to $1.4\overline{L_b}$—an order-of-magnitude smaller than $L_A$ of ~$20\overline{L_b}$ for the Madagascan rivers (Figure 3a). Furthermore, there is not an abrupt floodplain gradient break at the avulsion locations in the longitudinal swath profiles of the Madagascan rivers (Figure S4)—a key prediction of the geometric hypothesis that causes channel superelevation to be maximized at the avulsion sites (Figure 1b).

## 6. Discussion

Our results demonstrate that delta avulsion lengths in Madagascar are significantly longer than the backwater lengthscale (Figure 3a) and the estimated backwater and drawdown lengths, which contrast with observations of avulsions in low-gradient deltas (Chatanantavet et al., 2012; Ganti et al., 2014; Jerolmack & Swenson, 2007; Moodie et al., 2019). However, our results demonstrate that $L_A$ scales with the theoretical flood scour length for all natural deltas (Figure 3c). Under the backwater hypothesis, river drawdown during

floods causes bed scour within the lowermost reaches of coastal rivers that drives the fluvial system out of equilibrium (Chatanantavet & Lamb, 2014; Lamb et al., 2012), resulting in a preferential aggradation zone that produces avulsions upstream of the flood scour zone (Figure 1c; Chatanantavet et al., 2012; Ganti, Chadwick, Hassenruck-Gudipati, Fuller, et al., 2016; Ganti, Chadwick, Hassenruck-Gudipati, & Lamb, 2016). The river drawdown zone can be approximated to first order by the backwater lengthscale (Lamb et al., 2012), and $L_A \sim \overline{L_b}$ for most rivers because $\overline{L_b}$ approximates the flood-induced scour length. However, the flood-induced scour length can deviate significantly from $\overline{L_b}$ under certain conditions, and by accounting for the typical flood duration relative to the channel bed adjustment time scale, Equation 2 provides a more complete framework to estimate $l_{scour}$ beyond the simplistic assumption of $l_{scour} \sim \overline{L_b}$ (Ganti et al., 2019). For rivers with low gradients and long $t_{adj}$, typical floods result in $T_e^* < 1$ such that flood scours and avulsions are limited to the backwater zone (Chadwick et al., 2019). This prediction is consistent field observations of bed scour within the lowermost ~100 km reach of the Mississippi (Nittrouer et al., 2012) ($l_{scour} = 93 \pm 38$ km; Figure 3c), and the location of two major lobe-scale avulsions on the Lower Mississippi river ($T_e^* \sim 10^{-3}$; Figure 3b) that occurred 490 km (0.5 to 0.3 ka; $L_A \approx \overline{L_b}$) and 75–125 km (1.4 to 1.0 ka; $L_A = 0.16\overline{L_b} - 0.27\overline{L_b}$) upstream of the shoreline (Chamberlain et al., 2018). Similarly, in the backwater-scaled physical experiment with $T_e^* = 0.36$ (Figure 3b; Ganti, Chadwick, Hassenruck-Gudipati, Fuller, et al., 2016; Ganti, Chadwick, Hassenruck-Gudipati, & Lamb, 2016), flood-induced scours were limited to the backwater zone (Figure 3a), and $L_A \approx l_{scour}$ (Figure 3c). In contrast, in fine-grained sediment dispersal systems with unusually high sediment loads (Ma et al., 2017, 2020), like the Madagascan rivers, $t_{adj}$ can be short such that typical floods can have $T_e^* > 1$ and produce erosional scours with $l_{scour} > \overline{L_b}$ (Figure 3c; Ganti et al., 2019) and consequently $L_A > \overline{L_b}$ (Figure 3a; Chadwick et al., 2019).

Results demonstrate that $L_A = (3.1 \pm 1.5) l_{scour}$ for the avulsion compilation on natural deltas, which contrasts with the observation of $L_A \approx l_{scour}$ in the physical experiment (Ganti, Chadwick, Hassenruck-Gudipati, Fuller, et al., 2016; Ganti, Chadwick, Hassenruck-Gudipati, & Lamb, 2016) with deterministic flood frequency and magnitude (Figure 3c). These results indicate that Equation 2 only provides a lengthscale over which flood-induced scours occur in coastal rivers, and should be considered as a first-order estimate of $L_A$. The location of maximum riverbed aggradation over multiple flood cycles is likely a function of how the magnitude and frequency of floods covary, and the temporal sequence of floods may also play an important role. For example, temporally clustered floods can cause the amalgamation of bed scours that produce longer flood scour lengths than predicted by Equation 2. Further work is needed to test the universality of the scaling factor between $L_A$ and $l_{scour}$ for deltas across multiple climate zones, basin depths, and bed material grain sizes.

In contrast to the backwater hypothesis, if avulsions were triggered by the geometric mechanism, they should have occurred at a distance of about $\overline{L_b}$ upstream of the shoreline (Equation 3), which is inconsistent with field observations (Figure 3a). There is not a mechanism yet identified that would allow geometric avulsions to occur so far upstream because they are tied to the geometry of a prograding lobe (Figure 1b). For the Madagascan avulsions to be consistent with the geometric hypothesis, the rivers would require an unrealistic avulsion threshold of 20 (Equation 3), implying that the channel superelevation needed to trigger an avulsion is 20 channel depths—an inference that is inconsistent with field and flume studies with $h^*$ of the order of unity (Ganti et al., 2014, 2019; Mohrig et al., 2000). In addition, for wave-dominated deltas, the river mouth progradation is suppresed by wave erosion (Ratliff, 2017; Ratliff et al., 2018) such that $D_p \neq 20\overline{L_b}$.

Our results bolster the notion that delta lobe size is sensitive to the prevailing flood regime (Chadwick et al., 2019; Chatanantavet et al., 2012; Ganti, Chadwick, Hassenruck-Gudipati, Fuller, et al., 2016; Ganti, Chadwick, Hassenruck-Gudipati, & Lamb, 2016). Dam infrastructure in alluvial rivers affect the flood duration and bed material grain size and consequently influence $T_e^*$ of coastal rivers. Upstream changes that lead to prolonged floods or an increase in the fine fraction of bed material load can shift avulsion locations farther upstream (Equation 2). Furthermore, human-induced climate change is projected to vary flood frequency worldwide (Best & Darby, 2020; Hirabayashi et al., 2013), which will not only impact the global flooding risk from inundation of urban areas but can also shift the locus of avulsion sites on deltas, further exacerbating the flooding hazards for densely populated deltas.

## 7. Conclusions

Our results provide field testing of the backwater hypothesis for avulsions where natural flood discharge variability is a primary determinant of the lobe-scale avulsion sites on deltas. Analysis of historical avulsions in Madagascar indicates that the correlation between avulsion length and backwater lengthscale emerges only when the typical flood duration is shorter than the channel bed adjustment time scale ($T_e^* < 1$), consistent with previous backwater-influenced flume experiments and low-gradient coastal rivers. In contrast, steep rivers with fine bed sediment can have short channel bed adjustment time scales such that typical floods have $T_e^* > 1$. In such a scenario, flood-induced scours caused by backwater hydrodynamics can traverse the entire backwater zone and result in avulsions that are significantly farther upstream than backwater lengthscale. We find that avulsion lengths are $3.1 \pm 1.5$ times the theoretical flood scour lengths, highlighting the fundamental role of flood discharge variability in setting delta avulsion location.

## Data Availability Statement

Data sets used in this research are publicly available, with USGS/NASA Landsat satellite imagery and SRTM 1 arcsec elevation data downloaded from the USGS Earth Explorer (https://earthexplorer.usgs.gov/) and Sentinel 2 imagery downloaded from the Copernicus Open Access Hub (https://scihub.copernicus.eu/), river discharge data from the RivDIS and GRDC global discharge data sets (GRDC, 2015; Vorosmarty et al., 1998) were downloaded from or requested from https://doi.org/10.3334/ORNLDAAC/199 and https://www.bafg.de/GRDC, respectively, with surface water masks provided by the JRC Global Surface Water 1984–2018 data sets (Pekel et al., 2016) downloaded from https://global-surface-water.appspot.com/download. Representative global compilation of low gradient avulsions were compiled from previously published studies (Chatanantavet et al., 2012; Ganti et al., 2014, 2019; Jerolmack & Mohrig, 2007; Jerolmack & Swenson, 2007; Moodie et al., 2019). Tabular data for this study have been provided in the supporting information. All code and data used in this study can be downloaded from these sites (https://doi.org/10.6084/m9.figshare.12948671 and https://gitlab.com/sambrooke/avulsion-flood-scour-paper/-/releases/v1.2).

**Acknowledgments**
We thank R. C. Mahon for constructive comments on the manuscript. This work was supported by the National Science Foundation EAR 1935669 grant to Ganti and EAR 1427262 to Lamb.

## References

Ashton, A. D., & Giosan, L. (2011). Wave-angle control of delta evolution. *Geophysical Research Letters*, *38*, L13405. https://doi.org/10.1029/2011GL047630

Best, J., & Darby, S. E. (2020). The pace of human-induced change in large rivers: Stresses, resilience, and vulnerability to extreme events. *One Earth*, *2*(6), 510–514. https://doi.org/10.1016/j.oneear.2020.05.021

Blair, T. C., & McPherson, J. G. (1994). Alluvial fans and their natural distinction from rivers based on morphology, hydraulic processes, sedimentary processes, and facies assemblages. *Journal of Sedimentary Research*, *64*(3a), 450–489.

Bresse, J. A. C. (1860). *Cours de mécanique appliquée: Professé a l'École Imperiale des Ponts et Chaussées. Seconde partie, hydraulique*. Mallet-Bachelier, Paris, France: Gauthier-Villars.

Bresson, Y. (1956). *Mesures de transports solides sur le Mangoky au Banian*. Antananarivo, Madagascar: Institut de Recherche Scientifique de Madagascar.

Bull, W. B. (1977). The alluvial-fan environment. *Progress in Physical Geography*, *1*(2), 222–270. https://doi.org/10.1177/030913337700100202

Chadwick, A. J., Lamb, M. P., & Ganti, V. (2020). Accelerated river avulsion frequency on lowland deltas due to sea-level rise. *Proceedings of the National Academy of Sciences*, *117*(30), 17,584–17,590. https://doi.org/10.1073/pnas.1912351117

Chadwick, A. J., Lamb, M. P., Moodie, A. J., Parker, G., & Nittrouer, J. A. (2019). Origin of a preferential avulsion node on lowland river deltas. *Geophysical Research Letters*, *46*, 4267–4277. https://doi.org/10.1029/2019GL082491

Chamberlain, E. L., Törnqvist, T. E., Shen, Z., Mauz, B., & Wallinga, J. (2018). Anatomy of Mississippi delta growth and its implications for coastal restoration. *Science Advances*, *4*, eaar4740. https://doi.org/10.1126/sciadv.aar4740

Chatanantavet, P., & Lamb, M. P. (2014). Sediment transport and topographic evolution of a coupled river and river plume system: An experimental and numerical study. *Journal of Geophysical Research: Earth Surface*, *119*, 1263–1282. https://doi.org/10.1002/2013JF002810

Chatanantavet, P., Lamb, M. P., & Nittrouer, J. A. (2012). Backwater controls of avulsion location on deltas. *Geophysical Research Letters*, *39*, L01402. https://doi.org/10.1029/2011GL050197

Cox, R., Bierman, P., Jungers, M. C., & Rakotondrazafy, A. F. M. (2009). Erosion rates and sediment sources in Madagascar inferred from $^{10}$Be analysis of lavaka, slope, and river sediment. *The Journal of Geology*, *117*(4), 363–376. https://doi.org/10.1086/598945

Cox, R., Zentner, D. B., Rakotondrazafy, A. F. M., & Rasoazanamparany, C. F. (2010). Shakedown in Madagascar: Occurrence of lavakas (erosional gullies) associated with seismic activity. *Geology*, *38*(2), 179–182. https://doi.org/10.1130/G30670.1

Dunne, K. B. J., & Jerolmack, D. J. (2018). Evidence of, and a proposed explanation for, bimodal transport states in alluvial rivers. *Earth Surface Dynamics*, *6*(3), 583–594. https://doi.org/10.5194/esurf-6-583-2018

Fick, S. E., & Hijmans, R. J. (2017). WorldClim 2: New 1-km spatial resolution climate surfaces for global land areas. *International Journal of Climatology*, *37*(12), 4302–4315. https://doi.org/10.1002/joc.5086

Ganti, V., Chadwick, A. J., Hassenruck-Gudipati, H. J., Fuller, B. M., & Lamb, M. P. (2016). Experimental river delta size set by multiple floods and backwater hydrodynamics. *Science Advances*, *2*(5), e1501768. https://doi.org/10.1126/sciadv.1501768

Ganti, V., Chadwick, A. J., Hassenruck-Gudipati, H. J., & Lamb, M. P. (2016). Avulsion cycles and their stratigraphic signature on an experimental backwater-controlled delta. *Journal of Geophysical Research: Earth Surface*, *121*, 1651–1675. https://doi.org/10.1002/2016JF003915

Ganti, V., Chu, Z., Lamb, M. P., Nittrouer, J. A., & Parker, G. (2014). Testing morphodynamic controls on the location and frequency of river avulsions on fans versus deltas: Huanghe (Yellow River), China. *Geophysical Research Letters*, *41*, 7882–7890. https://doi.org/10.1002/2014GL061918

Ganti, V., Lamb, M. P., & Chadwick, A. J. (2019). Autogenic erosional surfaces in fluvio-deltaic stratigraphy from floods, avulsions, and backwater hydrodynamics. *Journal of Sedimentary Research*, *89*(8), 815–832. https://doi.org/10.2110/jsr.2019.40

Gibling, M. R. (2006). Width and thickness of fluvial channel bodies and valley fills in the geological record: A literature compilation and classification. *Journal of Sedimentary Research*, *76*(5), 731–770. https://doi.org/10.2110/jsr.2006.060

GRDC (2015). Global and Madagascar monthly and daily river discharge data. The Global Runoff Data Centre, 56068 Koblenz, Germany.

Hartley, A. J., Weissmann, G. S., & Scuderi, L. (2017). Controls on the apex location of large deltas. *Journal of the Geological Society*, *174*(1), 10–13. https://doi.org/10.1144/jgs2015-154

Hirabayashi, Y., Mahendran, R., Koirala, S., Konoshima, L., Yamazaki, D., Watanabe, S., et al. (2013). Global flood risk under climate change. *Nature Climate Change*, *3*(9), 816–821. https://doi.org/10.1038/nclimate1911

Jerolmack, D. J. (2009). Conceptual framework for assessing the response of delta channel networks to Holocene Sea level rise. *Quaternary Science Reviews*, *28*(17-18), 1786–1800. https://doi.org/10.1016/j.quascirev.2009.02.015

Jerolmack, D. J., & Mohrig, D. (2007). Conditions for branching in depositional rivers. *Geology*, *35*(5), 463–466. https://doi.org/10.1130/G23308A.1

Jerolmack, D. J., & Swenson, J. B. (2007). Scaling relationships and evolution of distributary networks on wave-influenced deltas. *Geophysical Research Letters*, *34*, L23402. https://doi.org/10.1029/2007GL031823

Jones, H. L., & Hajek, E. A. (2007). Characterizing avulsion stratigraphy in ancient alluvial deposits. *Sedimentary Geology*, *202*(1-2), 124–137. https://doi.org/10.1016/j.sedgeo.2007.02.003

Jones, L. S., & Schumm, S. A. (1999). Causes of avulsion: An overview. In *Fluvial sedimentology VI* (pp. 169–178). Oxford: Blackwell.

Kidder, T. R., & Liu, H. (2017). Bridging theoretical gaps in geoarchaeology: Archaeology, geoarchaeology, and history in the Yellow River valley, China. *Archaeological and Anthropological Sciences*, *9*(8), 1585–1602. https://doi.org/10.1007/s12520-014-0184-5

Lamb, M. P., Nittrouer, J. A., Mohrig, D., & Shaw, J. (2012). Backwater and river plume controls on scour upstream of river mouths: Implications for fluvio-deltaic morphodynamics. *Journal of Geophysical Research*, *117*, F01002. https://doi.org/10.1029/2011JF002079

Ma, H., Nittrouer, J. A., Naito, K., Fu, X., Zhang, Y., Moodie, A. J., et al. (2017). The exceptional sediment load of fine-grained dispersal systems: Example of the Yellow River, China. *Science Advances*, *3*, e1603114. https://doi.org/10.1126/sciadv.1603114

Ma, H., Nittrouer, J. A., Wu, B., Lamb, M. P., Zhang, Y., Mohrig, D., et al. (2020). Universal relation with regime transition for sediment transport in fine-grained rivers. *Proceedings of the National Academy of Sciences*, *117*(1), 171–176. https://doi.org/10.1073/pnas.1911225116

Mohrig, D., Heller, P. L., Paola, C., & Lyons, W. J. (2000). Interpreting avulsion process from ancient alluvial sequences: Guadalope-Matarranya system (northern Spain) and Wasatch formation (western Colorado). *Geological Society of America Bulletin*, *112*(12), 1787–1803. https://doi.org/10.1130/0016-7606(2000)112%3C1787:IAPFAA%3E2.0.CO;2

Moodie, A. J., Nittrouer, J. A., Ma, H., Carlson, B. N., Chadwick, A. J., Lamb, M. P., & Parker, G. (2019). Modeling deltaic lobe-building cycles and channel avulsions for the Yellow River Delta, China. *Journal of Geophysical Research: Earth Surface*, *124*, 2438–2462. https://doi.org/10.1029/2019JF005220

Moran, K. E., Nittrouer, J. A., Perillo, M. M., Lorenzo-Trueba, J., & Anderson, J. B. (2017). Morphodynamic modeling of fluvial channel fill and avulsion time scales during early Holocene transgression, as substantiated by the incised valley stratigraphy of the Trinity River, Texas. *Journal of Geophysical Research: Earth Surface*, *122*, 215–234. https://doi.org/10.1002/2015JF003778

Nassor, A., & Jury, M. R. (1997). Intra-seasonal climate variability of Madagascar. Part 2: Evolution of flood events. *Meteorology and Atmospheric Physics*, *64*(3-4), 243–254. https://doi.org/10.1007/BF01029696

Nassor, A., & Jury, M. R. (1998). Intra-seasonal climate variability of Madagascar. Part 1: Mean summer conditions. *Meteorology and Atmospheric Physics*, *65*(1–2), 31–41. https://doi.org/10.1007/BF01030267

Nienhuis, J. H., Ashton, A. D., Edmonds, D. A., Hoitink, A. J. F., Kettner, A. J., Rowland, J. C., & Törnqvist, T. E. (2020). Global-scale human impact on delta morphology has led to net land area gain. *Nature*, *577*(7791), 514–518. https://doi.org/10.1038/s41586-019-1905-9

Nittrouer, J. A., Shaw, J., Lamb, M. P., & Mohrig, D. (2012). Spatial and temporal trends for water-flow velocity and bed-material sediment transport in the lower Mississippi River. *GSA Bulletin*, *124*(3–4), 400–414. https://doi.org/10.1130/B30497.1

Paola, C. (2000). Quantitative models of sedimentary basin filling. *Sedimentology*, *47*, 121–178. https://doi:10.1046/j.1365-3091.2000.00006.x

Paola, C., & Mohrig, D. (1996). Palaeohydraulics revisited: Palaeoslope estimation in coarse-grained braided rivers. *Basin Research*, *8*(3), 243–254. https://doi.org/10.1046/j.1365-2117.1996.00253.x

Pekel, J., Cottam, A., Gorelick, N., & Belward, A. (2016). High-resolution mapping of global surface water and its long-term changes. *Nature*, *540*(7633), 418–422. https://doi.org/10.1038/nature20584

Randrianarijaona, P. (1983). The erosion of Madagascar. *Ambio*, *12*(6), 308–311. Retrieved from JSTOR

Ratliff, K. M. (2017). From the river to the sea: Modeling coastal river, wetland, and shoreline dynamics. Retrieved from https://dukespace.lib.duke.edu/dspace/handle/10161/14458

Ratliff, K. M., Hutton, E. H. W., & Murray, A. B. (2018). Exploring wave and sea-level rise effects on delta morphodynamics with a coupled river-ocean model. *Journal of Geophysical Research: Earth Surface*, *123*, 2887–2900. https://doi.org/10.1029/2018JF004757

Reitz, M. D., Pickering, J. L., Goodbred, S. L., Paola, C., Steckler, M. S., Seeber, L., & Akhter, S. H. (2015). Effects of tectonic deformation and sea level on river path selection: Theory and application to the Ganges-Brahmaputra-Meghna River Delta. *Journal of Geophysical Research: Earth Surface*, *120*, 671–689. https://doi.org/10.1002/2014JF003202

Sinha, R. (2009). The great avulsion of Kosi on 18 August 2008. *Current Science*, *97*(3), 429–433.

Slingerland, R., & Smith, N. D. (2004). River avulsions and their deposits. *Annual Review of Earth and Planetary Sciences*, *32*(1), 257–285. https://doi.org/10.1146/annurev.earth.32.101802.120201

Syvitski, J. P. M., & Brakenridge, G. R. (2013). Causation and avoidance of catastrophic flooding along the Indus River, Pakistan. *GSA Today*, *23*(1), 4–10. https://doi.org/10.1130/GSATG165A.1

Syvitski, J. P. M., Kettner, A. J., Overeem, I., Hutton, E. W. H., Hannon, M. T., Brakenridge, G. R., et al. (2009). Sinking deltas due to human activities. *Nature Geoscience*, *2*(10), 681–686. https://doi.org/10.1038/ngeo629

Syvitski, J. P. M., & Saito, Y. (2007). Morphodynamics of deltas under the influence of humans. *Global and Planetary Change*, *57*(3-4), 261–282. https://doi.org/10.1016/j.gloplacha.2006.12.001

Törnqvist, T. E. (1994). Middle and late Holocene avulsion history of the river Rhine (Rhine-Meuse delta, Netherlands). *Geology*, *22*(8), 711–714. https://doi.org/10.1130/0091-7613(1994)022%3C0711:MALHAH%3E2.3.CO;2

Trampush, S. M., Huzurbazar, S., & McElroy, B. (2014). Empirical assessment of theory for bankfull characteristics of alluvial channels. *Water Resources Research*, *50*, 9211–9220. https://doi.org/10.1002/2014WR015597

Trower, E. J., Ganti, V., Fischer, W. W., & Lamb, M. P. (2018). Erosional surfaces in the upper cretaceous Castlegate sandstone (Utah, USA): Sequence boundaries or autogenic scour from backwater hydrodynamics? *Geology*, *46*(8), 707–710. https://doi.org/10.1130/G40273.1

Unruh, J., McConnell, B., & Rodman, J. (2010). Environmental change and adaptation in degraded agro-ecosystems: The case of highland Madagascar. *Area*. https://doi.org/10.1111/j.1475-4762.2009.00928.x

Voarintsoa, N. R. G., Cox, R., Razanatseheno, M. O. M., & Rakotondrazafy, A. F. M. (2012). Relation between bedrock geology, topography and lavaka distribution in Madagascar. *South African Journal of Geology*, *115*(2), 225–250. https://doi.org/10.2113/gssajg.115.225

Vorosmarty, C. J., Fekete, B. M., & Tucker, B. A. (1998). Global river discharge, 1807-1991, V[ersion]. 1.1 (RivDIS). *ORNL DAAC*.

Walling, D. E. (1984). *The sediment yields of African rivers*, *IAHS-AISH Publication* (Vol. 144, pp. 265–283). Wallingford, United Kingdom: IAHS Press.

Wells, N. A., & Andriamihaja, B. (1993). The initiation and growth of gullies in Madagascar: Are humans to blame? *Geomorphology*, *8*(1), 1–46. https://doi.org/10.1016/0169-555X(93)90002-J

World Bank, USAID, Cooperation Suisse, UNESCO; UNDP, & World Wildlife Fund (1988). Madagascar—Environmental action plan (Environmental Action Plan. Vol. 1. Report E21). Retrieved from The World Bank website: http://documents.worldbank.org/curated/en/970001468773368889/Madagascar-Environmental-action-plan